The 3C-6H polytypic transition in SiC as revealed by diffuse x-ray scattering

Alexandre Boulle, J. Aubé, I. Galben-Sandulache, D. Chaussende

▶ **To cite this version:**

Alexandre Boulle, J. Aubé, I. Galben-Sandulache, D. Chaussende. The 3C-6H polytypic transition in SiC as revealed by diffuse x-ray scattering. Applied Physics Letters, 2009, 94 (20), pp.201904. 10.1063/1.3141509 . hal-02190246

HAL Id: hal-02190246
https://hal.science/hal-02190246

Submitted on 22 Jul 2019

HAL is a multi-disciplinary open access archive for the deposit and dissemination of scientific research documents, whether they are published or not. The documents may come from teaching and research institutions in France or abroad, or from public or private research centers.

L'archive ouverte pluridisciplinaire **HAL**, est destinée au dépôt et à la diffusion de documents scientifiques de niveau recherche, publiés ou non, émanant des établissements d'enseignement et de recherche français ou étrangers, des laboratoires publics ou privés.

The 3*C*-6*H* polytypic transition in SiC as revealed by diffuse x-ray scattering

A. Boulle,[1,a)] J. Aube,[1] I. G. Galben-Sandulache,[2] and D. Chaussende[2]
[1]*Science des Procédés Céramiques et de Traitements de Surface CNRS UMR 6638, ENSCI, 47 avenue Albert Thomas, 87065 Limoges Cedex, France*
[2]*Laboratoire des Matériaux et du Génie Physique CNRS UMR 5628, Grenoble INP, Minatec, 3 parvis Louis Néel, BP 257, 38016 Grenoble Cedex 01, France*

(Received 18 March 2009; accepted 1 May 2009; published online 22 May 2009)

The 3*C*-6*H* polytypic transition in SiC single crystals is studied by means of diffuse x-ray scattering. Based on numerical simulations of the diffuse scattering intensity distribution we unambiguously prove that the 3*C*-6*H* transition in SiC occurs through the glide of partial dislocations and not by the "layer displacement" mechanism (i.e., local diffusional rearrangement of the Si and C atoms). The technique is extremely sensitive and can be used as a nondestructive mean to obtain statistically relevant values of the transition level down to ~0.05%. © *2009 American Institute of Physics*. [DOI: 10.1063/1.3141509]

Cubic silicon carbide (3*C*-SiC) is a wide-band-gap semiconductor of high interest for high power, high frequencies, and harsh environments operating devices. Important efforts have therefore been directed to optimizing the growth conditions of 3*C*-SiC films,[1] characterizing their electronic[2] and structural[3,4] properties. However, despite decades of studies, the crystalline quality of 3*C*-SiC single crystals is too poor to allow their effective integration in electronic devices. Bulk growth of high quality 3*C*-SiC ingots still is an issue as the high temperatures required to grow SiC (>1900 °C) usually promote the solid-state 3*C*-6*H* polytypic transition through the formation of a large number of planar defects (mainly stacking faults, SFs).[5] Even if recent attempts could pave the way of 3*C*-SiC bulk growth,[6] a thorough study of such a transition is one of the key for a real development of 3*C*-SiC material.

Up until now, the mechanism involved in the 3*C*-6*H* transition in SiC single crystals is still not clearly identified. This question has been first tackled by Jagodzinski[7] and Krishna and Marshall[8] both using x-ray diffraction photographs. Both studies concluded that the transition occurs in the solid-state through a "layer displacement" mechanism where two 3*C* sequences, *ABCA*[*BC*], are transformed into a 6*H* sequence, *ABCA*[*CB*], by local diffusional rearrangement of the Si and C atoms in the two last layers (indicated by the square brackets). Contradictory results have been obtained by Pirouz and Young[9] using high-resolution transmission electron microscopy. They suggested that the transformation occurs through the glide of partial dislocations, so that the initial regular stacking is successively transformed into *ABCA*|*CA* and *ABCAC*|*B* (the staking fault associated with the partial is indicated by the bar). The 3*C*-6*H* transition in SiC single crystals has also been investigated using Raman scattering,[10] although no direct information regarding the transformation mechanism could be obtained by this technique. In this letter we report on high-resolution diffuse x-ray scattering (DXS) experiments performed on 3*C*-SiC single crystals undergoing the 3*C*-6*H* polytypic transition. First, with the aid of numerical simulations, we show that the analysis of experimental DXS intensity distributions allows an unambiguous determination of the mechanism involved in the 3*C*-6*H* transition. Second, contrarily to the techniques mentioned above, we demonstrate that the quantitative comparison of experimental DXS profiles with numerical simulations allows to straightforwardly obtain the transformation level.

In the present study, three different samples are analyzed. All crystals are 10×10 mm^2, 250-μm-thick, (001)-oriented 3*C*-SiC provided by HAST Corporation. The first sample (sample 1) is a high quality (i.e., untransformed) 3*C*-SiC crystal. Sample 2, is a low quality sample where the 3*C*-6*H* transition occurred during crystal growth. Finally, sample 3 is of the same type than sample 2 and has been annealed at 1700 °C during 5 h in order to promote the transformation. DXS experiments were conducted on a laboratory equipment mounted on a high power x-ray source coupled with a four reflections Ge(220) monochromator and equipped with a curved position sensitive detector (PSD).[11] The x-ray beam is 100 μm thick and 10 mm wide. Maps of the scattered intensity including the (002) and (113) reflections of 3*C*-SiC were recorded for each sample (Fig. 1). A schematic representation of the scattering geometry and the area scanned in the reciprocal space is shown in Fig. 1(f).

The map corresponding to sample 1 [Fig. 1(a)] exhibits two intense and narrow spots corresponding to the (002) and (113) reflections of 3*C*-SiC. The magnification of the (002) reflection [Fig. 1(d)] reveals that the reflections are streaked along directions making an angle $\psi\approx55°$ with the $[001]_c$ direction (the subscript *c* stands for cubic), which is the signature of the presence of SFs lying in the {111} planes ($\psi_{(111),(001)}=54.74°$). The streaks are symmetric with respect to the center of the reflection and their intensity is relatively weak which indicates a low density of randomly distributed SFs.[4] On the contrary, in the map corresponding to sample 2 [Figs. 1(b) and 1(e)] the streaks extend throughout wide regions of the reciprocal space and their intensity is much more pronounced. Finally, in the map corresponding to sample 3 [Fig. 1(c)] there is an intense and inhomogeneous streak of diffuse intensity joining the (002) and the (113) reflections. In terms of the equivalent hexagonal axes[12] (i.e.,

a)Electronic mail: alexandre.boulle@unilim.fr.

 © 2009 American Institute of Physics

Author complimentary copy. Redistribution subject to AIP license or copyright, see http://apl.aip.org/apl/copyright.jsp

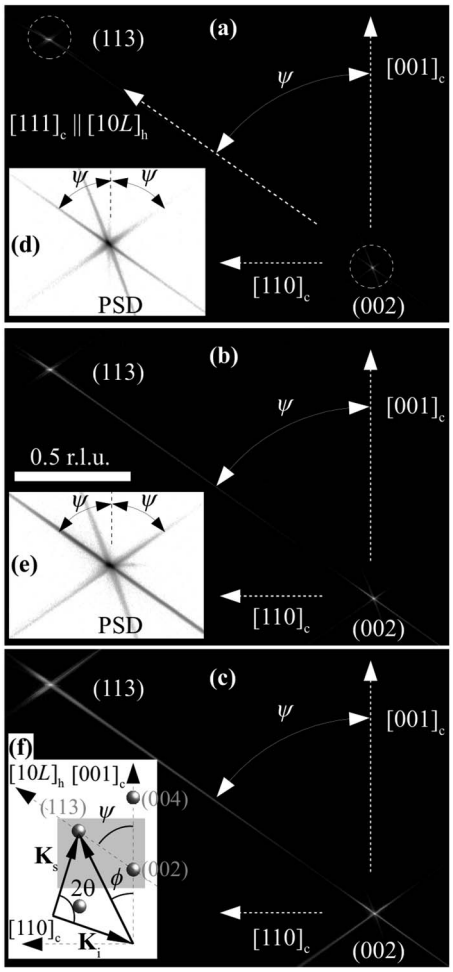

FIG. 1. Reciprocal space maps including the (002) and (113) reflections of 3*C*-SiC corresponding to sample 1 (a), sample 2 (b), and sample 3 (c). The scale bar, shown in (b), is given reciprocal lattice units (i.e., in units of *hkl*). For sample 1 the reflections are indicated by the dashed circles. Insets (d) and (e) are 12× magnifications in reversed contrast of the (002) reflection evidencing the diffuse streaks. The streak labeled "PSD" is due to the transmittance function of the PSD. In all cases the intensity is plotted logarithmically. Inset (f) is a schematic representation of the scattering geometry. The area scanned in reciprocal space is shown as the gray rectangle and the spheres correspond to the reflections of 3*C*-SiC. $\mathbf{K}_i$ and $\mathbf{K}_s$ are the wave vectors of the incident and the scattered radiation.

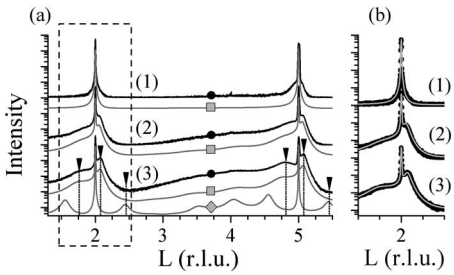

FIG. 2. (a) Intensity distribution along the $[10L]_h$ row. The labels (1–3) correspond to sample 1–3, respectively. The black curves (black circles) correspond to the experimental data. The gray curves are the calculated intensity profiles with the dislocation-based model (squares) and the layer displacement model (diamond). The curves are shifted vertically for clarity. The dashed arrows indicate features in the diffuse scattering structure that are perfectly reproduced with the dislocation-based model and that the layer displacement model fails to reproduce. (b) Enlarged view of the $L=1.5-2.5$ region evidencing the quality of the simulation (black circles: experimental data; gray line: simulation with the dislocation model).

$[001]_h \parallel [111]_c$ and $[100]_h \parallel [-110]_c$) the streak direction corresponds to the $[10L]_h$ direction, where $L=2$ and $L=5$ for the (002) and (113) reflections, respectively. The increase in the DXS intensity together with its inhomogeneous character suggests a high density of planar defects that are nonrandomly distributed throughout the crystal, i.e., the 3*C*-SiC crystal is probably partly transformed.

The intensity distribution in the diffuse streak [black curves, Fig. 2] clearly shows an increase in the DXS intensity as well as an inhomogeneous distribution of this intensity when moving from sample (1) to sample (3). These profiles have been interpreted with the help of numerical simulations of the scattered intensity. It must be emphasized that when L is varied from 1.5 to 5.5, the corresponding 2θ angle spans an $\sim 42°$ range so that all θ-dependent terms have to be correctly be taken into account. In the framework of the kinematical scattering theory[12] the intensity distribution along the $[10L]_h$ row can be written

$$I(L) = k\delta V(\theta)L(\theta)P(\theta)\int dL' R(L')I_s(L-L') + b, \qquad (1)$$

where the scale factor k and the background b are constants for a given set of experimental conditions (incident beam intensity, counting time, etc.). $\delta V(\theta)$ is the variation of the irradiated volume during the experiment, and writes $\sin(\theta+\phi)/[\sin(\theta+\phi)+\sin(\theta-\phi)]$, where ϕ is the angle between [001] and any point along the $[10L]_h$ row [see Fig. 1(f)]. $L(\theta)=1/\sin 2\theta$ is the Lorentz factor and $P(\theta)$ is the polarization factor, which, using a four reflections Ge(220) monochromator, can be written $(1+\cos^8 \theta_{\mathrm{Ge}(220)} \cos^2 \theta)/2$. $R(L)$ is the resolution function of the diffractometer. In the present case it has the shape of a Gaussian function the width of which can be precisely evaluated.[11] Finally, $I_s(L)$ is the intensity scattered from the sample. This term contains the information regarding the stacking sequence in the crystal and is therefore sensitive to the mechanism involved in the transition.

Within the formalism of Kabra *et al.*[13] the intensity distribution along the $[10L]_h$ row in a partly transformed crystal can be written

$$I_t(L) = C|f_0|^2 I_c + 2(1-C)|f_0|^2 \times \Re\left\{\frac{1}{2} + \frac{\sum_{n=1}^{N-1}\sum_{m=0}^{n-1} a_{N-m}J_{n-m}\exp[-2\pi i(N-n)L/3] - a_0 J_0}{\sum_{n=0}^{N} a_n \exp[-2\pi i n L/3]}\right\}. \qquad (2)$$

The first term on the right-hand side of Eq. (2) is the coherent part of the scattered intensity, the intensity of which is modulated by a Debye–Waller—like factor $(C \in [0,1])$ which depends on the faulting structure and the defect density. The coherent intensity I_c depends on the size and shape of the crystalline domains over which diffraction is coherent (mosaic domains).[14] It turned out that finite size effects could be safely neglected here, so that in the following the mosaic domains have been assimilated to cubes with dimensions (6 μm) much larger than the diffractometer coherence length. f_0 is the structure factor of a single "SiC" layer. The second term on the right-hand side of Eq. (2) is the diffuse scattering due to the presence of faults. Both J_m (the pair

Author complimentary copy. Redistribution subject to AIP license or copyright, see http://apl.aip.org/apl/copyright.jsp

correlation function) and a_n (the coefficients of the "characteristic equation") can be calculated analytically assuming a certain transition mechanism and therefore a particular faulting structure. For the dislocation-based mechanisms it comes $C=0$, $N=6$; the expression of J_m and a_n are given in Ref. 13 (p. 1657) and solely depends on the transformation level, τ. For the layer displacement mechanism, $C=[(1+2\tau)/(1+5\tau)]^2$ and $N=5$. The expressions of J_m and a_n are not given in Ref. 13. We derived the coefficients and obtained $\tau\omega^2$, $\tau\omega$, τ, $\tau\omega^2$, $\tau\omega$ and 1 for a_0 to a_5, respectively [$\omega=\exp(2\pi i/3)$]. For J_m we obtained $J_0=[6\omega^2\tau+3\tau^2(1+\omega+8\omega^2)]/D$, $J_1=[-3\omega^2\tau+3\tau^2(\omega-4\omega^2-2)]/D$, $J_2=[3\tau^2(1-\omega)^2]/D$, $J_3=[3\tau^2(1+\omega-2\omega^2)]/D$, $J_4=[3\tau^2(\omega+\omega^2-2)]/D$, and $D=\omega^2(1+5\tau^2)$.

An important assumption made in deriving Eq. (2) is that the whole crystal is transformed *simultaneously*. However, considering the very large lateral dimensions of the crystals (10×10 mm^2) this is very unlikely to happen. Moreover this assumption is contradictory with the analysis of the transformation using Raman scattering[10] which proved that the transformation is initiated at the surface and then propagates into the crystal volume. In the volume probed with the x-ray beam both transformed and untransformed areas certainly coexist so that we finally write the intensity scattered from the sample as

$$I_s = x_t I_t + (1 - x_t) I_c, \tag{3}$$

where x_t is the volume fraction of transformed material.

The best simulation results [using Eqs. (1)–(3)] obtained for the dislocation-based model (square) and the layer displacement model (diamond) are shown in Fig. 2. Let us first consider the data corresponding to sample 3. The major result of this analysis is that the dislocation-based model fits the DXS intensity distribution over the whole investigated L-range. On the contrary, the layer displacement model clearly fails to reproduce the observed data. This simple result provides an unambiguous proof that the 3C-6H transition occurs through the glide of partial dislocations and not by local diffusional rearrangement of the Si and C atoms. The relevance of this result can be attested by the inspection of the enlarged view of the (002) reflection [Fig. 2(b)]: the model perfectly fits the data over approximately four orders of magnitude whereas there are only two fitting parameters (the transformation level τ and the volume fraction x_t) for the whole angular range considered. It must be emphasized that although the same theoretical basis is used, this result is opposite to the conclusions of Kabra *et al.*[13] This discrepancy can be explained by the fact that their study was based on the analysis of x-ray photographs. This prevented them to access the fine structure of the diffuse scattering which is yet mandatory to clearly distinguish the different mechanisms [see Fig. 2(a), sample 3]. The overall transformation level $\tau\times x_t$ is straightforwardly obtained from the simulation procedure. We obtain 0.05%, 1.6%, and 4.3% for sample 1–3, respectively, which shows that even a very low transformation level produce significant effects in terms of diffuse scattering.

In summary, the interpretation of the diffuse x-ray scattering allowed us to prove unambiguously that the 3C-6H transition in SiC occurs through the glide of partial dislocations. Moreover, this method is non destructive and provides averaged, statistically relevant measurements the transition level. A detailed knowledge of this polytypic transition in SiC will be of great help for the development of high quality and high performance 3C-SiC materials and devices.

The authors thank the French ANR-Jeunes Chercheurs program (Contract No. ANR-05-JCJC-0207-01) and the MANSiC—Marie Curie Research and Training Network (Contract No. MRTN-CT-2006-035735) for their financial supports.

[1] A. Fissel, B. Schröter, U. Kaiser, and W. Richter, Appl. Phys. Lett. **77**, 2418 (2000).
[2] A. Fissel, W. Richter, J. Furthmüller, and F. Bechstedt, Appl. Phys. Lett. **78**, 2512 (2001); K.-B. Park, Y. Ding, J. P. Pelz, P. G. Neudeck, and A. Trunek, *ibid.* **89**, 042103 (2006); M. V. S. Chandrashekhar, C. I. Thomas, J. Liu, and M. G. Spencer, *ibid.* **91**, 033503 (2007).
[3] M. Zielinski, A. Leycuras, S. Ndiaye, and T. Chassagne, Appl. Phys. Lett. **89**, 131906 (2006); C. Coletti, C. L. Frewin, S. E. Saddow, M. Hetzel, C. Virojanadara, and U. Starke, *ibid.* **91**, 061914 (2007); R. Anzalone, C. Bongiorno, A. Severino, G. D'Arrigo, G. Abbondanza, G. Foti, and F. La Via, *ibid.* **92**, 224102 (2008).
[4] A. Boulle, D. Chaussende, L. Latu-Romain, F. Conchon, O. Masson, and R. Guinebretière, Appl. Phys. Lett. **89**, 091902 (2006).
[5] N. W. Jepps and T. F. Page, Prog. Cryst. Growth Charact. **7**, 259 (1983).
[6] D. Chaussende, F. Mercier, A. Boulle, F. Conchon, M. Soueidan, G. Ferro, A. Mantzari, A. Andreadou, E. K. Polychroniadis, C. Balloud, S. Juillaguet, J. Camassel, and M. Pons, J. Cryst. Growth **310**, 976 (2008).
[7] H. Jagodzinski, Kristallogr. **16**, 1235 (1971).
[8] P. Krishna and R. C. Marshall, J. Cryst. Growth **11**, 147 (1971).
[9] P. Pirouz and J. W. Yang, Ultramicroscopy **51**, 189 (1993).
[10] W. S. Yoo and H. Matsunami, J. Appl. Phys. **70**, 7124 (1991); R. Püsche, M. Hundhausen, L. Ley, K. Semmelroth, F. Schmid, G. Pensl, and H. Nagasawa, *ibid.* **96**, 5569 (2004).
[11] A. Boulle, O. Masson, R. Guinebretière, A. Lecomte, and A. Dauger, J. Appl. Crystallogr. **35**, 606 (2002).
[12] B. E. Warren, *X-ray Diffraction* (Addison-Wesley, New-York, 1969), pp. 46 and 258.
[13] V. K. Kabra, D. Pandey, and S. Lele, J. Mater. Sci. **21**, 1654 (1986).
[14] A. Boulle, R. Guinebretière, and A. Dauger, J. Phys. D: Appl. Phys. **38**, 3907 (2005).

Author complimentary copy. Redistribution subject to AIP license or copyright, see http://apl.aip.org/apl/copyright.jsp